



MMAN4951 - Research Thesis A

Interim Report and Project Plan

Investigation of the aerodynamics of wings with leading-edge serrations

Author: Jordan Whittaker¹

Supervisor: Con Doolan

UNSW Sydney, School of Mechanical & Manufacturing Engineering

April 28, 2025

Abstract

This research project investigates the aerodynamic performance of wings with leading-edge (LE) serrations inspired by the tubercles on humpback whale flippers. LE serrations have been shown to delay stall, enhance lift, and reduce drag in lift device's high angle of attack (AoA) regimes, making them invaluable in high-performance applications such as military aircraft, UAVs, wind turbines, and rotors. This project conducts a parametric computational study on the geometric properties of LE serrations varying shape, amplitude, wavelength, and termination distance verified against wind tunnel experiments. The aim is to characterise how the properties of LE serrations affect aerodynamic performance and to optimise for the optimal configurations. This report outlines the current literature, the project aims, a proposed investigation methodology, preliminary serratation designs, and CFD simulations.

¹jordan.whittaker@student.unsw.edu.au

Nomenclature

A_F	Axial force
A	Amplitude of serrations
C_D	Drag coefficient
C_L	Lift coefficient
c	Mean chord
D	Drag force
d	Termination distance of serrations
L	Lift force
N_F	Normal force
q_∞	Free-stream dynamic pressure
Re	Reynolds number
s	span
V_∞	Free-stream flow velocity
α	Angle of attack
λ	Wavelength of serrations
ρ_∞	Free-stream density
AoA	Angle of attack
CFD	Copmutational fluid dynamics
DES	Detached eddy simulation
DNS	Direct numerical simulation
SST	Educational wind tunnel
LES	Large eddy simulation
LE	Leading-edge
OC	Optimal configuration
SST	Shear stress transport

1 Introduction

Leading-edge (LE) serrations are well known to enhance the aerodynamic performance of wings and reduce noise production from interaction with turbulent flow. The motivation for these investigations into LE serrations on wings is biological. Evolution is a powerful optimiser; thus, mimicking animal morphologies in design can be highly beneficial. Humpback whales (*Megaptera novaeangliae*) have large sinusoidal serrations denoted as tubercles on the leading-edge (LE) of their pectoral flippers seen in Figure 1. They were first hypothesised by Fish and Battle (1995) [6] to contribute to their high hydrodynamic manoeuvrability. The aerodynamic effect of LE serrations has been heavily investigated, and an observed increase in performance, specifically in the high AoA regime. The vortices created by the tubercles are hypothesised to delay flow detachment by re-energising the boundary layer and creating stable low-pressure regions on the wing's top surface. This can delay flow separation, increase stall angle, and lift in stall and post-stall regimes.



Figure 1: Sinusoidal LE tubercles of a humpback whale's (*Megaptera novaeangliae*) flipper.

Increasing manoeuvrability and stall performance on wings and other lift structures has many applications within high-performance aircraft. Most aircraft-specific investigations in LE serrations are conducted on UAVs [2, 24] as UAVs often operate at high angles of attack (AoA) and in highly turbulent environments where the likelihood of stall is great. Wind turbines often operate in off-design conditions, including yawed flow and unsteady wind conditions where effective AoA is highly variable. The stall-improving measures of LE serrations are highly effective in widening their effective operating range and, therefore, energy production. A similar effect is seen in helicopter rotors where LE serrations have been known to reduce the impact of static and dynamic stall [3], and this extends to applications of fans, drones and other rotational lift devices.

This report will investigate the current literature on LE serrations and propose a project plan for the current calendar year to explore the aerodynamic properties of LE serrations and the variable effect of their geometric properties. Section 2 reviews the current literature on LE serrations, followed by the identification of project aims and the proposed research question. The proposed methodology and timeline for the investigation are outlined in Section 3, followed by the current progress of the project in Section 4.

2 Literature Review

2.1 Biological inspiration for LE serrations

Humpback whales (*Megaptera novaeangliae*) have sinusoidal protrusions on the LE of their pectoral flippers known as tubercles. These protrusions are hypothesised to improve hydrodynamic performance and enable high-AoA manoeuvres. First investigated by Fish and Battle [6] in 1995, their unique flipper morphology delays flow separation, delays stall and enhances lift through the generation of streamwise vortices that energise the boundary layer and suppress spanwise flow separation. Miklosovic et al. [18] provided the first experimental validation of these effects by testing serrated leading edges on scaled wing models. Their results demonstrated a stall delay of up to 40%, an increase in the maximum lift coefficient, and a substantial reduction in post-stall drag. These findings sparked the development of biomimetic leading-edge serrations and tubercle-inspired modifications in aerospace and turbomachinery applications, where controlling flow separation and stall is critical.

2.2 Scope of current LE sertation investigations

LE serrations are periodic protrusions that occur on the LE of a wing. In the current literature, many different geometries and study environments have been tested, varying the airfoil, Reynolds number, sertation shape/profile, wavelength, amplitude and, minimally, the sertation termination distance. This study will focus on 2D airfoils, where chord, c , and airfoil profile do not change across the span of the wing. The aerodynamics of the relevant studies will be discussed in Section 2.3; this section will define the ranges of the investigated serrations to determine value limits for further investigation.

2.2.1 Profile/shape

The profile/shape of the sertation defines its 2D protrusion profile that varies across studies. Most relevant studies within the current literature investigate a sinusoidal sertation profile [1–5, 8–19, 21–26] seen in Figure 2a similar to that of the humpback whale. Other minimally investigated profiles are a "wavy" sinusoidal sertation in Hansen (2012) [8] seen in Figure 2c where the apex of the sertation is varied vertically instead of horizontally and a triangular profile [4, 12, 17, 19] seen in Figure 2b. A "sawtooth"-like sertation profile is commonly investigated in aeroacoustic studies, mimicking the LE serrations seen in Owls. The dimensions of the serrations seen on owls are significantly smaller compared to tubercle studies but, for illustrative purposes, have been scaled in Figure 2d to similar dimensions. No significant aerodynamic papers investigate this profile, but most aeroacoustic investigations control for C_L and C_D and find a minimal aerodynamic effect.

2.2.2 Wavelength

Variations in the wavelength, λ , of the LE serrations have been extensively explored throughout the literature, typically presented as the non-dimensional quantity λ/c . The wavelength parameter λ is dimensioned in Figure 3. The range of wavelengths investigated in the literature is $0.016 \leq \lambda/c \leq 1$; however, no study investigates near the full range of values. At the lower end of this range, Ke et al. (2002) [13] investigated five wavelengths in the range of $0.016 \leq \lambda/c \leq 0.064$ on an S809 airfoil,

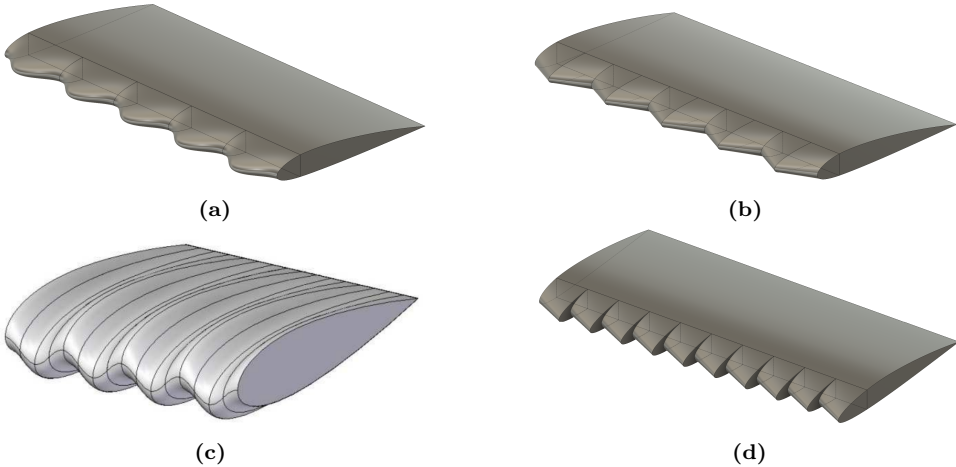


Figure 2: a) Sinusoidal serration profile, b) Triangular serration profile, c) "wavy" sinusoidal serration profile [8], d) "sawtooth"-like serration profile.

investigating the performance effect on wind turbines. Lacagnina et al. (2021) investigated three wavelengths in the range of $0.1 \leq \lambda/c \leq 0.3$ on a NACA 65(12)-10 airfoil, Zhaoyu We et al. (2019) [25] who investigated two wavelengths in the range of $0.25 \leq \lambda/c \leq 0.5$ on a NACA 634-021 airfoil gave insight into mid-range wavelengths. Manideep et al. (2022) [11] investigated two longer wavelength values in the range of $0.5 \leq \lambda/c \leq 1$ on a Wortmann FX 60-126 airfoil.

2.2.3 Amplitude

Variations in the LE serrations' amplitude, A , have also been extensively investigated throughout the literature. Most studies will preserve the planform area of the studied wing across amplitudes by letting the nominal chord length be the position of half amplitude. This can be seen in Figure 3. The amplitude in most studies is presented as the non-dimensional quantity A/c . The range of amplitudes investigated in the literature is $0.01 \leq \lambda/c \leq 0.3$; however, similar to the investigations of wavelengths, no study investigates near the full range of values. Notable comparative studies are done by He et al. (2023) [9] who investigated 4 amplitudes in the range of $0.025 \leq \lambda/c \leq 0.1$ on a NACA 634-021 airfoil, Ke et al.(2002) [13] who investigated 5 amplitudes in range of $0.01 \leq \lambda/c \leq 0.055$ on a S809 airfoil and Stalnov & Chong (2019) [22] who investigated 3 amplitudes in the range of $0.05 \leq \lambda/c \leq 0.5$ on a NACA 65(12)-10 airfoil. The overlap of these studies is difficult to analyse as the serraton's performance is highly dependent on study type and geometry. This will be further discussed in Section 2.3.

2.2.4 Termination distance

The serraton property investigated the least is the termination distance of the serraton, d , seen in Figure 3. No reviewed study varied the termination distance of the serrations, but most studies chose one of two values to be held constant or were unspecified. $1/3c$ and c where the most common termination distances seen in [3, 9, 10, 14, 22, 25] and [1, 2, 4, 5, 11, 13, 21, 26] respectively, with two other studies minimising termination distance and 6 unspecified.

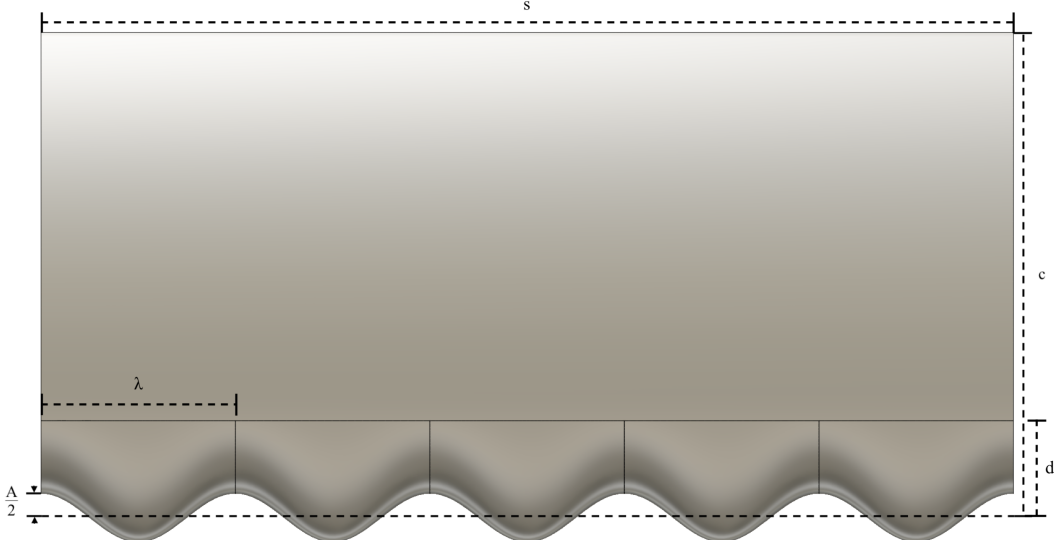


Figure 3: Parameter dimensions of a sinusoidal LE serrated airfoil including A = amplitude, λ = wavelength, d = termination distance, c = mean chord, S = span.

2.2.5 Airfoil

The variation in airfoil profile across studies depends on the wing type a study is investigating. A few of the studies directly investigated and verified the efficacy of serrations mimicking the humpback whale and thus used an airfoil profile similar to that of its flipper. The most common whale-like airfoil used is the cambered NACA 634-021 [9, 24, 25], which mimics the bulbous profile of the whale. Among the studies that investigated the efficacy of serrations on aircraft wings, the most common airfoil profiles are the uncambered NACA 0008 [12], the NACA 0012 [16], the NACA 0015 [15, 19], the NACA 0020 [17, 18] and the NACA 0021 [1, 3, 8] airfoil profiles. General cambered aircraft wing profiles were less explicitly studied, with the only notable study by Fernandes et al. (2013) [5], who investigated the cambered NACA 2412 airfoil profile. A large number of studies investigated rotors where the most common airfoil profile investigated is the NACA 65(12)-10 [14, 22]. Most other investigations used specialised airfoil profiles tailored to their investigation type, namely UAVS, rotors and fans. Only a single study by Hansen (2012) [8] varied the airfoil profile in their investigation, using both NACA 65-021 and NACA 0021 airfoil profiles within minimal aerodynamic difference.

2.2.6 Reynolds Number

Although the range of Reynolds numbers studied was extensive, $2 \times 10^4 \leq Re \leq 2.26 \times 10^6$, the number of studies that varied Re across their serrated wings was limited. The most common Re 's investigated are in the range of $1 \times 10^5 \leq Re \leq 5 \times 10^5$, close to what humpback whales experience during their hydrodynamic maneuvers [18]. The most notable studies found are by Wang et al. 2024 [24] who studied a constant serratation geometry across 3 Re in the range of $2.6 \times 10^5 \leq Re \leq 6.3 \times 10^5$ and Lacagnina et al. (2021) [14] who studied a variation in serratation geometry across 3 Re in the range of $2 \times 10^5 \leq Re \leq 4 \times 10^5$. Most studies within the literature do not vary the Re within their investigation.

2.2.7 Parametric Studies

Most studies within the current literature do not investigate a wide range of geometric and study properties as the number of required test cases grows rapidly with increasing variation. This is especially relevant for computational studies that require individual simulations for every AoA. Across-study results are difficult to analyse as a lack of variable control decreases comparison efficacy, which is why full parametric studies are essential. The most applicable parametric study within the literature is conducted by Lacagnina et al. (2021) [14] who experimentally studied the complete combinations of $\lambda/c = 0.1, 0.2, 0.3$, $A/c = 0.03, 0.06, 0.12$, and $Re = 2 \times 10^5, 3 \times 10^5, 4 \times 10^5$ on a NACA 65(12)-10 airfoil for a total of 27 test cases. The study used a sinusoidal serration shape and a termination distance of $1/3c$, which were held constant across all test cases. The most applicable computational parametric study within literature is conducted by Sathyabhama and Sreejith (2022) [21], who computationally studied the complete combinations of $\lambda/c = 0.1, 0.21, 0.41$ and $A/c = 0.013, 0.027, 0.053$ on an E216 airfoil for a total of 9 test cases. The test cases were simulated for 8 AoA values; thus, 72 simulations were run. The study used a sinusoidal serration shape, an unspecified termination distance (most likely c) and a $Re = 1 \times 10^5$, which were constant across all test cases. The results of these studies will be heavily investigated in Section 2.3.

2.2.8 Computational methods

Most applicable studies within the current literature use a combination of CFD and experimental wind tunnel testing. This is primarily due to the inaccuracy of CFD models in predicting stall and post-stall effects.

Ali et al. (2024) [1] investigated the accuracy of certain Reynolds average Navier-Stokes (RANS) CFD turbulence models on LE serrated wings compared to the experimental results found in Hansen et al. (2011) [7]. The accuracy of $k-\omega$ Shear stress transport (SST), $k-\epsilon$ realisable, $(\gamma - Re_\theta)$ SST, Transition $k-k_l-\omega$ model and Stress- ω Reynolds Stress Model (RSM) models were investigated across 5 AoA's ranging from $0^\circ - 20^\circ$. The model with the highest accuracy across all AoAs is the RSM model, but this comes with a higher computational cost than the other models investigated. The $k-\omega$ SST model was a fantastic predictor of the stall and post-stall region but was limited in predicting the pre-stall region. The worst predictor across all AoAs is the Transition $k-k_l-\omega$ model. This is corroborated by Lohry et al. (2012) [17] who also concluded that $k-\omega$ SST model was successful in predicting experimental results from Miklosovic et al. (2004) [18]. No applicable study has compared Direct Numerical Simulation (DNS), Large Eddy Simulation (LES) or Detached Eddy Simulations (DES) to the mentioned RANS turbulence models, as these methods require significantly more computational work and are in rarer use for comparative studies. The most commonly used turbulence model within relevant computational studies is the $k-\omega$ SST model [2, 4, 9, 11, 13, 15, 17, 26], which supports the results from Ali et al. (2024) [1]. The $k-\epsilon$ model [5] and $(\gamma - Re_\theta)$ SST [21] are minimally used within literature. Liu et al. (2022) [16] utilised the LES model and Troll et al. (2021) [19] utilised the DES model since they extensively investigated the vorticity of the flow over LE serrations, of which eddy simulation models are necessary.

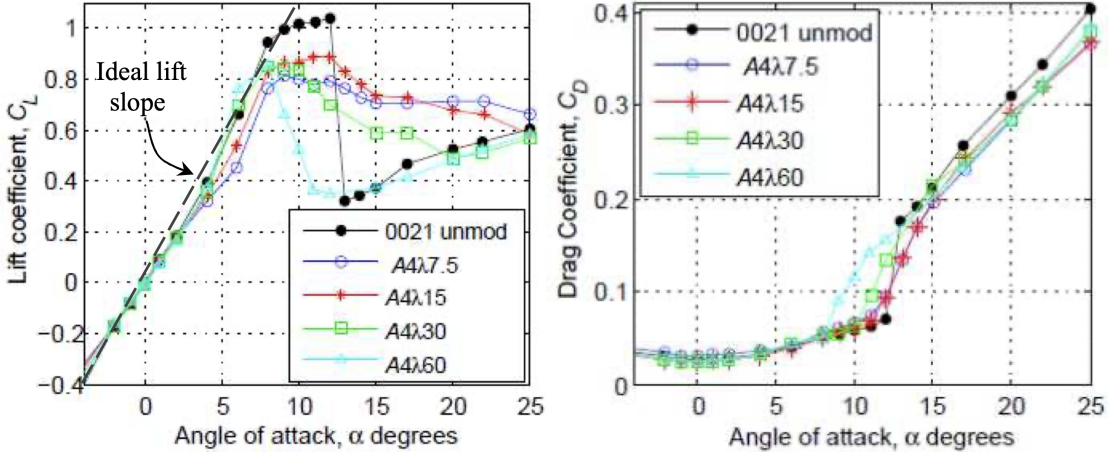


Figure 4: C_L and C_D vs α for various serration configurations seen in Figures 4.17 and 4.18 in Hansen (2012) [8].

2.3 Aerodynamic performance

2.3.1 Stall and post-stall characteristics

This section will analyse the results of the optimal configuration (OC) serrations found within the literature. The main aerodynamic change seen within current literature due to LE serrations is the wing's performance in the stall and post-stall regions. Nearly all studies see a dramatic increase in their post-stall lift coefficient, a reduction in stall angle and a "softer" stall profile compared to their baseline airfoil. As seen in Figure 4, the non-serrated lift coefficient curve dramatically drops during stall, but the curves representing the serrated wings exhibit a peak and continuous decrease in lift passing through stall. This is best demonstrated by Hansen (2012) [8], and this result is corroborated by Zhang et al. (2022) [26], Wei et al. (2019) [25] and Zhang et al. (2022) [26] who all denote this as the most significant effect of LE serrations on wings.

This softer stall profile dramatically increases the post-stall lift coefficient. While unanimous across all relevant literature, this effect ranges from a 6.7% [5] increase to a 100% [8] increase in their optimal serration configuration. Most results hover in the range of 14% – 35% [2, 14, 19, 22, 26] but the most significant results come from Borg et al. (2012) [3], Wei et al. (2019) [25] and Hansen (2012) [8] with a 80%, 70% and 100% increase in post-stall lift respectively. This is most likely due to these studies' extensive variable range, the average number of test cases of the three studies is 5, which gave sufficient parametrisation to optimise performance. As seen in Figure 4, the maximum increase in post-stall lift is generally located near the angle of non-serrated airfoil stall and slowly decreases as the angle of attack increases.

Most studies within the current literature report a decrease in the lift coefficient at stall and, thus, a decrease in the global maximum lift coefficient due to the introduction of LE serrations. This result is seen in the lift profiles in Figure 4. The difference in stall lift coefficients ranges in literature from -17% [3] to a 14% [2] with most results being within -17% to 0% [3, 8, 21, 24, 26]. The greatest increase in the stall lift coefficient within literature is an increase from the baseline airfoil of 40% by

Miklosovic et al. (2004) [18]. As this result has not been replicated again in literature and due to the specialised nature of the wing (mimicking a whale flipper), the result is taken as an outlier and thus is inapplicable.

Most studies within the current literature report a change in the stall angle due to the introduction of LE serrations, but the net effect is inconclusive. The literature exhibits a wide range of differences in stall angle from -6° [21] to 10° [2]. The average study reports a net 0° change in stall angle, with most results lying within $\pm 4^\circ$ [3, 5, 8, 14, 22, 25] of this value. The inconclusiveness of the resultant change in stall angle could be due to computational models' inaccuracy in predicting stall, despite both experimental and computational studies within the literature being reviewed.

Most studies within the current literature agree that introducing LE serrations decreases drag in the post-stall region, but this result is variable. In Borg (2012) [3], a 18% reduction in the coefficient of drag is exhibited in their optimal configuration, which is corroborated by Wei et al. (2019) [25] who saw a 25% reduction in post-stall drag and to a lesser degree seen in Hansen (2012) [8], Zhang et al. (2022) [26] and Sudhakar et al. (2017) [23] who all saw an approximate 5% decrease. Most other studies saw a negligible or slight increase in post-stall drag in their optimal configurations [2, 5, 11, 21] but the maximum reported increase in the coefficient of drag within the literature is Manideep et al. (2022) [11] who saw a 25% increase in post-stall drag. This results in a variable but a general increase in lift-to-drag ratio across literature in the post-stall region. The lift-to-drag ratio improvements range wildly from a reduction of 40% seen in Troll et al. (2021) [19], an almost negligible increase seen in Wei et al. (2019) [25] and Wang et al. (2024) [24], to an increase of 300% seen in Sudhakar et al. (2017) [23] in the post-stall region.

The geometries (explored further in Section 2.3.3) and study types explored within this section do not vary significantly, yet the results of each study do. While there are reported trends of aerodynamic change within the post-stall region, the primary outcome of this section is that the results vary wildly, and no single consensus on the aerodynamic effect in the post-stall region can be reached. The lack of consensus within the current literature indicates the need for more research into LE serrations.

2.3.2 Pre-stall characteristics

While some studies have shown minimal pre-stall improvements in aerodynamics, the consensus of the current literature is that there is a slight reduction in performance in the pre-stall regime of a LE serrated wing. As seen in Figure 4, the C_{L_α} and C_{D_α} gradients do not vary, but there is a constant reduction and increase in lift and drag coefficients, respectively, in the pre-stall region. This result is almost unanimously seen within the current literature.

2.3.3 Effects of serraton geometry

While extensively studied, the variable effect of serraton geometry is still relatively unknown. The whole parameter space of studied serraton geometries in the relevant literature is seen in Figure 5. While a cross-study comparison of serraton geometry effects is difficult, general trends arise. Most studies found that the smaller amplitude and larger wavelength serrations performed the best within their studied geometric ranges.

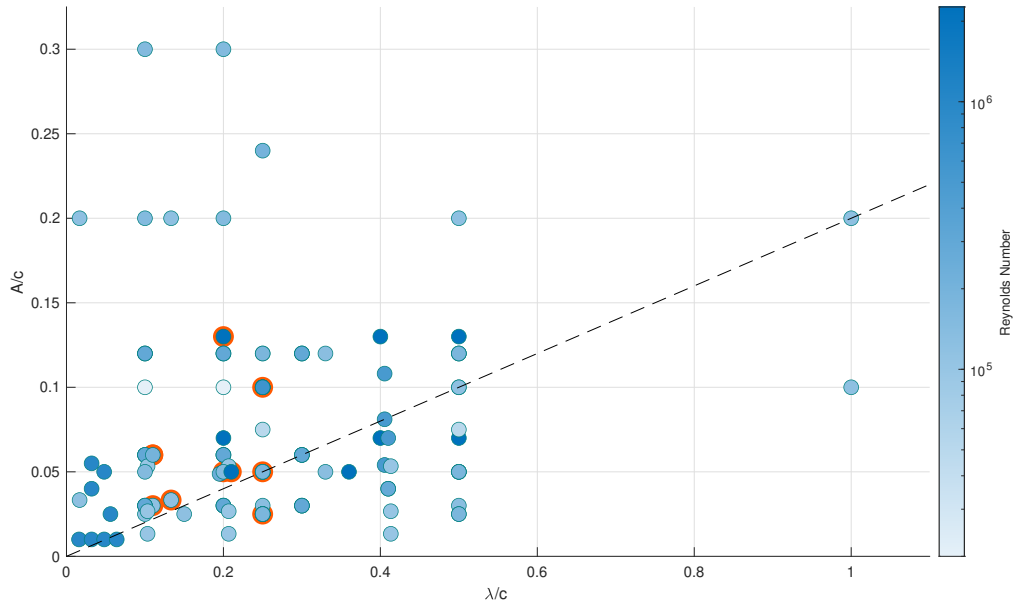


Figure 5: A scatter plot of all the currently researched serration configurations in terms of non-dimensional quantities λ/c , A/c and Re with optimal configurations (OC) for each reviewed study marked in red.

The optimal configuration (OC) amplitudes for most studies were $0.025c \leq A/c \leq 0.1c$ with the most common OC amplitude being $0.05c$. Hansen (2012) at OC $A/c = 0.03$ saw a significant decrease in stall angle, a decrease in post-stall lift, and a significant increase in drag around the stall point as the amplitude of the serrations increased, which can be seen in Figure 4. This result is strongly corroborated by Wei et al. (2019) [25], Zhang et al. (2022) [26] and Stanlov and Chang (2019) [22] who denote a sharp lift decrease and drag increase past $A/c > 0.3$. Denoted by Fernandes et al. (2013) [5], the lower amplitude serrations increased maximum post-stall lift but created a faster-decaying lift profile. This result is rare as most studies perceive a constant lift decay as amplitude increases. For most studies, their smallest tested amplitude is their best-performing configuration; thus, the effects of reducing the serration amplitude further are unknown. The pre-stall performance remained relatively constant as amplitude changed, with minor improvements as amplitude decreased.

The wavelengths of the OC for most studies were in the range of $0.15c \leq \lambda/c \leq 0.25c$ with the most common OC wavelength of $0.25c$. Fernandes et al. (2013) [5], Wei et al. (2019) [25] and Zhang et al. (2022) [26] all observed a constant decrease in lift, increase in drag and steeper post-stall lift decays for values of wavelengths that were less than $0.1c$ and greater than $0.35c$. The pre-stall performance remained relatively constant as amplitude changed with minor degradation in performance as wavelengths moved from the optimal range.

Wei et al. (2019) [25] observed that smaller amplitudes combined with smaller wavelengths performed optimally. They hypothesised that as amplitudes decrease and wavelengths increase, the serratation profile approaches that of an un-serrated wing, which nullifies the effects of the serratation. Borg

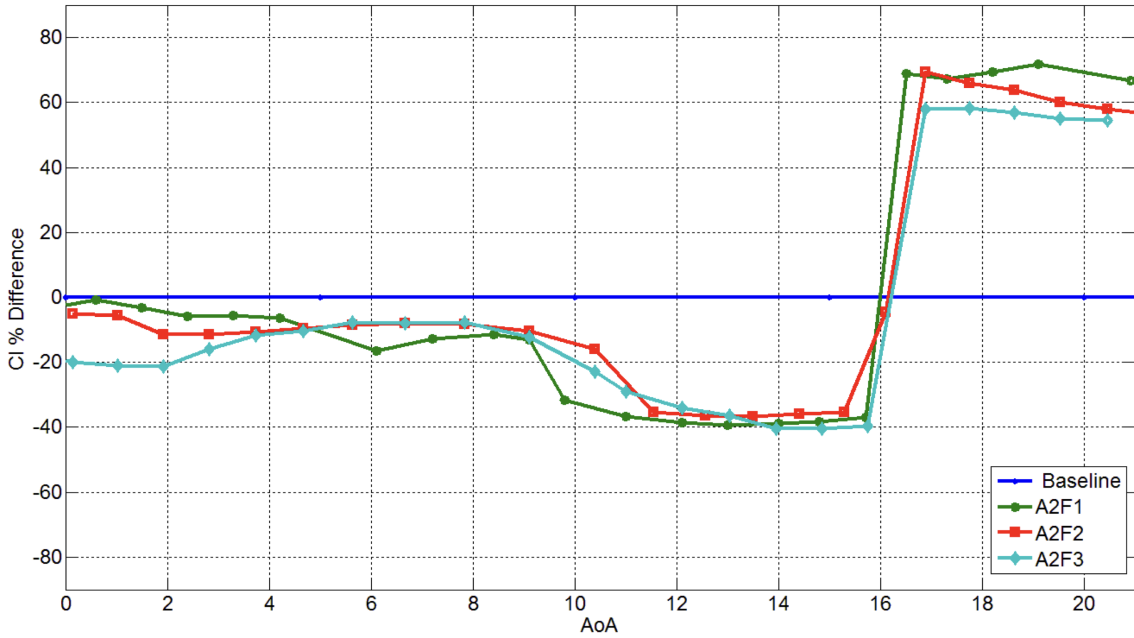


Figure 6: Graph showing the % difference in C_L of the investigated serration geometries to baseline wing in Figure 14 of Borg (2012) [3].

(2012) [3] observed that when a small amplitude is combined with a small wavelength, the increased surface disturbance degrades the flow, hypothesising an optimal balance of properties. The ratio λ/A is explored by Lacagnina et al. (2021) [14] who found the optimal ratio between 4 to 6. The line of constant $A/\lambda = 0.2$ ($\lambda/A = 5$) optimised in [14] is plotted in Figure 5 which approximately follows the trend of OCs observed. The existent but weak proportionality indicates other factors must be contributing to their aerodynamic performance, which are not controlled across studies.

No significant correlation of Re , airfoil, serration shape or termination distance is observed in the data collected across or within studies. A single study by Wang et al. (2024) [24] investigated the effect of changing Re , but there is no significant change to the aerodynamic parameters mentioned in this report.

2.3.4 Phenomenological principle

LE serrations alter the flow structures around the wing through targeted vortex generation and flow redistribution. The generated vortices are more stable structures than the general flow, allowing delayed flow separation through re-energising the boundary layer in those regions. Bardera et al. (2024) [2] observed the generation of counter-rotating vortex pairs along the leading edge, which suppresses the generation of laminar separation bubbles, which significantly increases flow attachment and thus improves lift. Laminar separation bubbles form at greater severity at higher AoAs. Therefore, serrations disproportionately increase the performance of airfoils post-stall. As explained in Manideep et al. (2022) [11], the cause of flow separation is a change in pressure gradient. There comes a point along

the wing where this pressure gradient drastically increases, and thus, flow separates. They hypothesised that the vortices generated by the LE serration disturb and "smooth" the drastic pressure increase, which degrades the pressure differential and delays flow separation. Wei et al. (2019) [25] hypothesised that each peak of a serration acts like a highly swept wing LE of a delta wing. This creates a strong streamwise vortex, much like a delta wing's LE vortex (LEV). There are other principles, including the inhibition of the spanwise progression of stall [7] and varying spanwise circulation [20], which are effects due to 3D airfoils which are out of the scope of this report.

2.4 Summary

The relevant literature on the effect of LE serrations is extensive, but there are several gaps in the observed research. The aerodynamic effect of LE serrations in the post-stall regime of a wing seen clearly in Figure 6 are the most promising advantage of their introduction, but the variability of the effects across studies introduces doubt to their overall efficacy. The minimal reduction in performance in the pre-stall region indicates that the serrations would be most efficiently used in high-manoeuvring aircraft and not in efficiency-optimised aircraft like passenger planes. The scope of the geometric properties that have been researched is extensive, with the effects of wavelength and amplitude approximately known. The most limited research is in comparative studies across all geometric properties, especially shape/profile and termination distance, where no relevant studies within the current literature were found.

3 Research Question and Project Plan

3.1 Research Question

Concluding from the literature review summary found in Section 2.4, the following research question is proposed;

How do the properties of leading-edge serrations affect the aerodynamic performance of wings?

3.2 Aims and Objectives

This project will answer the proposed research question by;

1. conducting a computational investigation into the properties of leading-edge serrations (shape, wavelength, amplitude, termination distance) optimising for aerodynamic performance (C_L , C_D , α_{stall}) across a range of AoA's and Re 's using computational fluid dynamic simulations,
2. verifying the trends of the computational investigation experimentally using the UNSW Educational Wind Tunnel (EWT).

3.3 Proposed Methodology

3.3.1 Computational investigation

3.3.1.1 Parameter space

As summarised in Section 2.4, the main gap in the current literature is the comparative effect of geometric properties of LE serrations, namely shape, wavelength, amplitude and termination distance. To answer the research question outlined in Section 3.1 and fill in the gaps in literature investigated in Section 2, the parameter ranges found in Table 1 will be investigated. Theoretically, this creates 60000 individual simulations across 1000 models, which is wildly unattainable and unnecessary (as some termination distances are incompatible with some amplitudes, this theoretical maximum is an overestimation). The initial approach to the computational study will investigate the variation in a single parameter, holding the other variables constant. The determination of the initial constants will be from the average of the optimised values found during the literature review in Section 2. The initial values are in Table 1.

Table 1: Paramter space

Paramter	Range	#	Initial Value
AoA, α ($^{\circ}$)	$[0, 30]$	15	—
Reynolds number, Re	$[5 \times 10^4, 1 \times 10^6]$	4	5×10^5
Shape/profile	Sinusoidal & Triangular	2	Sinusoidal
Amplitude, A/c	$[0.01, 0.3]$	10	0.05
Wavelength, λ/c	$[0.025, 0.5]$	10	0.2
Termination distance, d/c	$[0.1, 1]$	5	0.33

The first variable to be investigated will be the amplitude of the serrations. Ten different amplitude values will be investigated across 15 AoA's, holding the other variables constant. The optimised value for amplitude will be used for the subsequent variable investigations in the order of wavelength, termination distance, shape/profile and Reynolds number. This is, in total, 27 model investigations for a total of 405 individual simulations (if computationally sensible, Re will be run concurrently). This scope is attainable due to the use of UNSW's computational cluster Katana (further discussed in Section 3.3.1.4). The result of this initial investigation will show the general and variable effects of the investigated parameters on the aerodynamics of a LE serrated wing.

The second part of the computational investigation is the selective combination of variables. As discovered in Section 2.3.3, the parameter λ/A is essential in determining the aerodynamic performance of a LE serrated wing and thus a range of values will be investigated. Other possible combinations of variables are the parameter d/A , which explores how the severity of the serration's chord-wise perturbation of the wing affects aerodynamics and the combination of Re and shape/profile, which investigates how the characteristics of the flow interact with the geometry of the serration. The scope of the second part of the investigation is entirely determined by the number of simulations that can be run in the timeframe of the investigation.

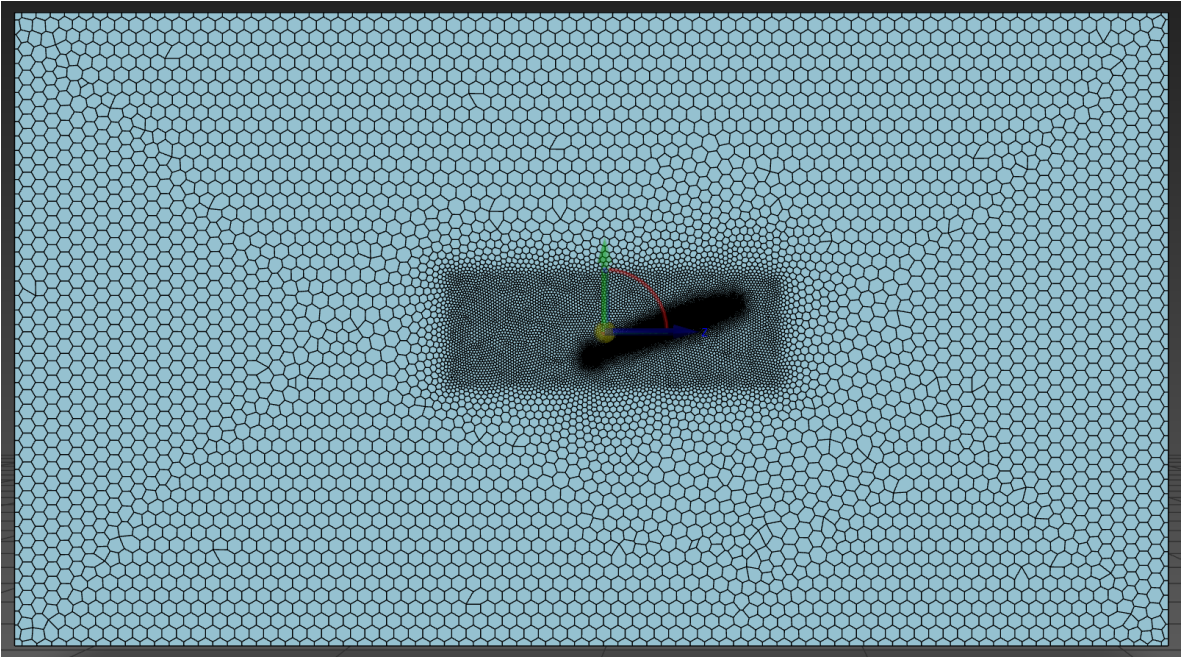


Figure 7: 3D cell mesh profile on the symmetry plane for a CFD study at an AoA of $\alpha = 25^\circ$.

3.3.1.2 Parametric CAD Model

The geometric properties of the wing will be parametrised within the CAD modelling software Fusion 360. The design of the parametrised wing is introduced in Section 4.1. This allows any set of parameters to be input and the subsequent serrated wing to be exported. Fusion 360 allows for the integration of Python APIs; thus, the range of serration combinations determined in Section 3.3.1.1 can be exported automatically and stored for subsequent importing into ANSYS Design Modeller.

3.3.1.3 ANSYS CFD Modelling

The most widely used and researched CFD model in the computational studies of LE serrations explored in Section 2.2.8 is the $k-\omega$ SST model. It is a good predictor of stall and is more computationally efficient than direct or eddy simulation methods; thus, it will be used in this study. The model is a two-equation eddy-viscosity turbulence model, and it blends the $k-\omega$ model near the wall with the $k-\epsilon$ model in the free stream. It has become an industry standard for the model's behaviour during adverse pressure gradients and flow separation, suitable for predicting flow in the post-stall region of this computational investigation.

The model will sit in the centre of a fluid domain. The necessary dimensions of the fluid domain have been optimised through preliminary CFD simulations, increasing the dimensions of the domain until the output of the simulations converges on a value. The dimensions of the box are $3c$ upstream of the model, $4c$ downstream of the model, $2c$ above and below the model, and $2c$ span-wise of the model (span-to-chord ratio of 2, further discussed in Section 4.1). The dimensions of the box may be refined to better mimic the dimensions of UNSW's Educational Wind Tunnel (EWT) if necessary. A

symmetry plane is used down the centre of the wing chord-wise to reduce computational work. The model has been designed such that all generated serrations will be symmetric down the centre of the wing chord-wise.

Through ANSYS Fluent meshing, the surface mesh of the models can be defined. The LE and the wing's body are two regions of the model that need local mesh refinements. Along the wing's LE, the serrations' geometry is highly curved. Thus, a curvature local mesh refinement is used to capture the geometry's complexity successfully. The curvature resolution is set to 7° with a minimum cell size of $0.0005c$ and a maximum cell size of $0.005c$. A proximity local mesh refinement is used on the wing's body, set to a Cells per Gap value of 2 with a minimum cell size of $0.0005c$ and a maximum cell size of $0.01c$. The global surface mesh is generated with a minimum cell size of $0.0005c$ and a maximum of $0.1c$. All surface mesh growth rates are set to 1.1 to capture regions of high variability. A rectangular prism region is defined around the model with dimensions extending 50% past the model geometry along all dimensions and 100% in the downstream path. This region is used as a local volume mesh to capture the highly variable flow along the top of the wing and in the wake. The region is variable with AoA to ensure its efficacy across all design points. The refinement sets a target volume mesh size of $0.02c$. A 6-layer smooth-transition boundary layer is defined on all surfaces of the wing with a transition ratio of 0.272 and a growth rate of 1.2. A global poly-hex-core volume mesh is generated for the fluid region with a minimum cell size of $0.0005c$ and a maximum cell size of $0.032c$. Depending on the complexity of the serrations, this creates a mesh with a cell number between 8,000,000 and 10,000,000. An image of the cell distribution can be seen in Figure 7. These values will be finalised before the commencement of the computational investigation.

3.3.1.4 Parametric studies on ANSYS

UNSW has access to the academic version of ANSYS, which allows for parametric studies within ANSYS Workbench. This includes the introduction of geometric parameters into Design Modeller and boundary conditions parameters within Fluent. The wing geometry will be designed and exported through Fusion 360, but the AoA of the model will be set up within ANSYS. A rotational transformation of the model around $1/2c$ will be determined by a parameter θ that can be set to a range of values within ANSYS Workbench. The inlet velocity will be set to a parameter V within ANSYS Fluent, which can also be varied within the parametric analysis mode of ANSYS Workbench. The study will set an AoA within the model domain, the domain will be meshed with the necessary surface mesh conditions, the inlet boundary conditions will be set, and the simulation will be run. This will be done for the set of AoAs and associated Re determined within Section 3.3.1.1. This can be set up within a single ANSYS Workbench project, and thus, despite the individual number of simulations per model of the order of $(\#AoA \times \#Re)$, the human input is minimal. The limitation is the wall time allowed per computation on UNSW's cluster Katana. The base maximum wall time is 12 hours per node, which is insufficient for a complete model study. Upon request, the maximum wall time per node can be increased (inquiries to increase wall time are ongoing) or if increasing wall time is unavailable, a single model study will be split into parts and simulated separately.

3.3.1.5 Computations on Katana

The computational work per model study is extensive; thus, UNSW's computational cluster Katana will be utilised to complete the simulations. The number of nodes available for this study is limited to the nodes controlled by the School of Mechanical and Manufacturing Engineering, and the number that can be run simultaneously will be determined through discussions with UNSW. Due to a data collection period of 5 months (timeline further outlined in Section 3.4), the necessary simultaneous node usage should be limited to ~ 10 . As mentioned in Section 3.3.1.1, the scope of the investigation will be determined by the number of simulations that can be run in that time. The cluster can be accessed through UNSW's Research Technology Services (ResTech) server on a local machine, and projects will be launched using the compatible TUI PuTTY. If necessary, this process can be automated locally using a Python script. The File Transfer Protocol (FTP) ability of the software FileZilla will be used to transfer the output data of the parametric studies stored on Katana to a local machine, where the lift and drag coefficients will be automatically imported as a CSV file to be analysed.

3.3.2 Experimental Verification - UNSW Educational Wind Tunnel

To assess the results of the computational investigation experimentally, selective serration geometries will be 3D printed and tested on the UNSW Educational Wind Tunnel (EWT). The aerodynamic forces are written by a sting balance located within EWT. The balance collects the model's normal forces (N_F) and the axial forces (A_F). The axis of the sting balance changes with changing AoA (α) and thus, for every AoA, the collected forces need to be transformed into lift (L) and drag (D) values through the following formulas;

$$L = N_F \cos \alpha - A_F \sin \alpha, \quad (1)$$

$$D = A_F \cos \alpha + N_F \sin \alpha. \quad (2)$$

The values for lift and drag can be transformed into their subsequent coefficients using the following formulas;

$$C_L = \frac{L}{q_\infty s}, \quad (3)$$

$$C_D = \frac{D}{q_\infty s}, \quad (4)$$

where the value for dynamic pressure is calculated by;

$$q_\infty = \frac{1}{2} \rho_\infty V_\infty^2. \quad (5)$$

3.3.3 Resources Required

The resources required to perform this investigation are;

- Aerodynamics Lab Access,
- Educational Wind Tunnel,

- 3D Printer,
- ANSYS Workbench, Design Modeler, SpaceClaim and Fluent,
- UNSW Katana Cluster,
- Fusion 360.

All necessary training and up-skilling have been completed for the determined required resources.

3.4 Project Timeline

The project's proposed timeline can be seen in Figure 11. The EWT mount will be designed (B1), and subsequent CFD testing will be concluded in the exam period, so design point modifications can be made if necessary. The fluid domain and mesh resolution determination (B2, B3) will be concluded during Term 1's exam period; thus, the first part of the computation investigation can commence within the Term 1 break. The first part of the computational investigation will extend through to the end of Term 2, giving ample time for computations and revision. Once the initial results are completed around Week 2 of Term 2, the 3D printing of model geometry (B6) will commence, and the experimental investigation (B7) will begin shortly after. Part 2 of the computational investigation (B5) will commence in week 6 of Term 2 after sufficient results have been reported to know what suitable parameter combinations should be investigated. Results analysis (B8) will be done concurrently throughout all investigations. After the Thesis B progress report has been written and submitted (B9, B10), the Thesis report (C1) will be started in the Term 2 break, a draft of which will be given to my supervisor in Week 6. After the completion of both experimental and computational investigations, additional data collection (C3) will be concluded in Term 3, Week 8 and final preparations for the presentation (C4) will be made before presenting (C6) in Week 11. The Thesis report will be submitted (C5) in Week 10 of Term 3.

4 Project Dependent Preparations

4.1 Preliminary Designs

The design of the LE serrated wing can be seen dimensioned in Figure 3. The model is designed in Fusion 360, and all geometric properties are set to parameters. Using the parametric analysis feature of Fusion 360, any set of values can be input, and the geometry is automatically changed. There were many design considerations during the creation of the model. From the results of Section 2.2.3, the amplitude has been designed such that the platform area is invariant under a change in serratation geometry. This is done by ensuring the mean chord, c , of the model, is the location of half amplitude. The wavelength of the model is created for a single cell and then is tiled in divisible units of the span across the LE of the wing. This ensures that the ends of the wings, across all serratation combinations, always end in minimum amplitude and are symmetric over half-span. The termination distance of the serratation determines how far along the chord the serratation perturbs the wing's surface. A section of the airfoil profile is scaled in the chord-wise direction to create the necessary amplitudes of the

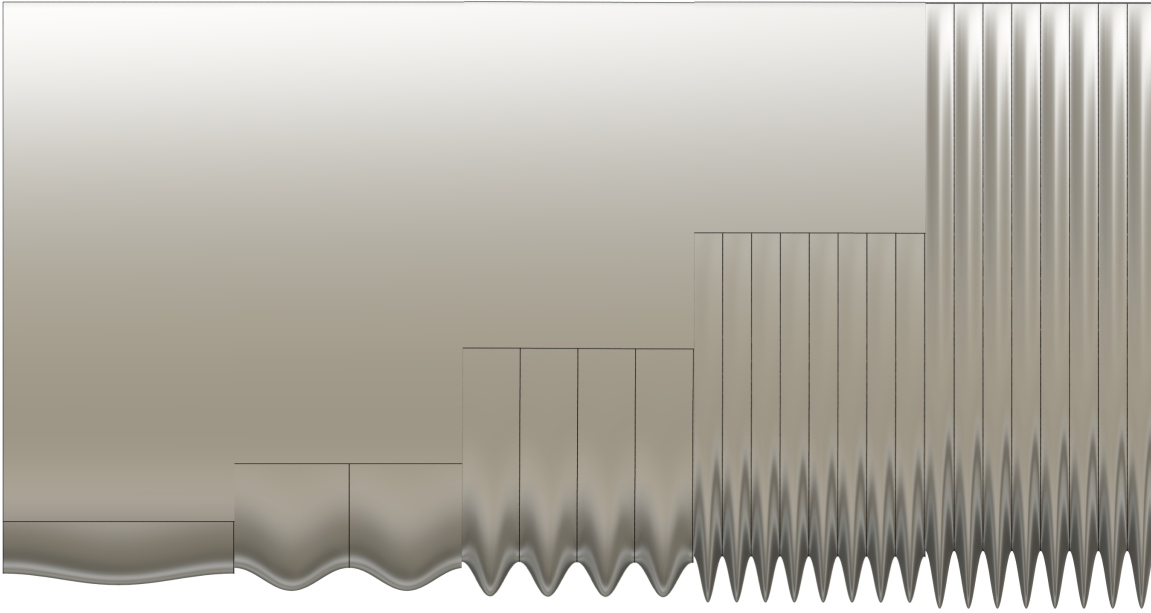


Figure 8: Image showing the evolution of geometric parameters of the parametric CAD model of the serrated wing. From left to right, showing decreasing wavelength, λ , increasing amplitude, A and increasing termination distance, d , for a sinusoidal serrat.

serration, and the point defining that section is the termination distance. The entire airfoil profile is scaled if the termination distance is set to c . Fusion 360 cannot create a perfect sinusoidal profile, and thus, the profile is estimated using the horizontal projection of a circle onto the span-wise geometry of the serrat. The triangular profile, seen in Figure 2b, is controlled by the ratio of λ and A , which determines the angle the triangular profile follows. The airfoil NACA 2412 is chosen due to the lack of direct investigation into non-specialised cambered airfoils investigated in Section 2.2.5. Figure 8 shows an image of the parameter variation. The value for the chord is modelled as $c = 1\text{ m}$ and span of $s = 2\text{ m}$ with a $s/c = 2$. This will be scaled for further CFD simulations to best represent the geometry and Re to be used experimentally.

An arm with a symmetric airfoil profile will extend from the bottom surface of the wing, attaching to a cylindrical tube that can mount to the sting balance in the EWT for experimental testing. The outer diameter of the sting balance mount is $3/8''$ or $\sim 9.5\text{ mm}$. The model-balance interface has yet to be designed. For 3D printing, the model will be split at the termination point of the serrat and attached post-print. This allows models with constant termination distance to reuse the wing's body for multiple serrat configurations.

4.2 Preliminary CFD

The majority of the preliminary CFD simulations have been used to determine the necessary mesh and fluid domain values, which are discussed in Section 3.3.1.3. Some preliminary results have been created, as shown in Figure 9. This initial investigation varied the flow velocity around a wing with the serrat geometry $\lambda/c = 0.1$, $A/c = 0.05$ and $d/c = 0.2$ compared to a non-serrated wing to determine

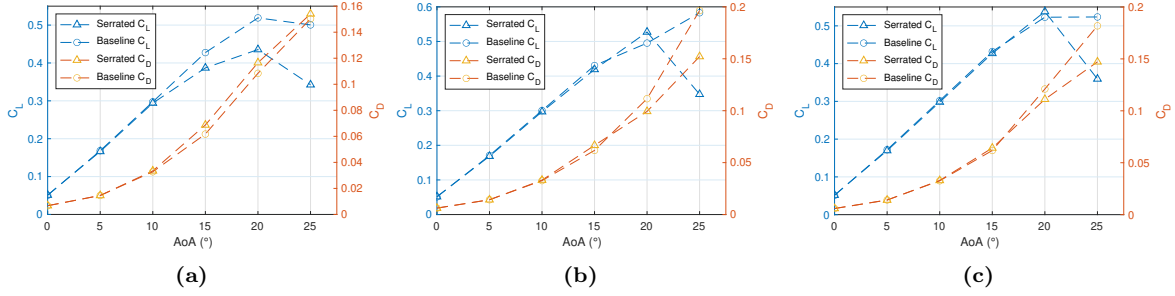


Figure 9: Lift and drag coefficients comparing a non-serrated baseline airfoil to a sinusoidal serrated airfoil with properties $\lambda/c = 0.1$, $A/c = 0.05$ and $d/c = 0.2$ with flow velocity of a) $V = 20 \text{ ms}^{-1}$ b) $V = 35 \text{ ms}^{-1}$ and c) $V = 50 \text{ ms}^{-1}$.

the need for investigations into Re and for a proof of concept of variable serration modelling. A total of 2 models were investigated across 6 AoAs and three flow velocities for a total of 24 simulations. This was conducted on three nodes of Katana using the methodology discussed in Section 3.3 and was completed in 5 hours. This initial testing confirmed the need for investigations into Re as there is significant performance variation across flow velocities. A velocity streamline map, seen in Figure 10, was created to verify the efficacy of the simulation in capturing the low-pressure region of the flow and wake which was successful.

4.3 Budget

All software and lab access are provided for free by UNSW. For the experimental investigation, many serration models will need to be 3D printed. For honours students, 3D printing is free for coursework. The number of the models required to be 3D printed is undetermined, but a non-conservative estimate is ~ 30 . For an estimated cost of \$5.50 a print at $15\times$ reduced scale of $133 \text{ mm} \times 67 \text{ mm}$, if it's needed to be personally funded, it would be an approximate \$165 cost for the 3D printing.

4.4 Safety Documentation and Training

The only safety documentation and training necessary for this project surrounds the use of the EWT in UNSW's Aerodynamic Lab. The relevant certifications are listed in Table 2.

Table 2: Relevant certifications for the use of the EWT and UNSW's Aerodynamics Lab

Certifications	Status
HSE orientation quiz	Completed
Safety@UNSW (SAFETYUNSW) Online Course	Completed
Lab Health and Safety (SAFETYLABS) Online Course	Completed
Hazardous Chemicals (SAFETYCHEM) Online Course	Completed
EWT Induction	Completed
UNSW 204 Aerodynamics Lab Access	Completed

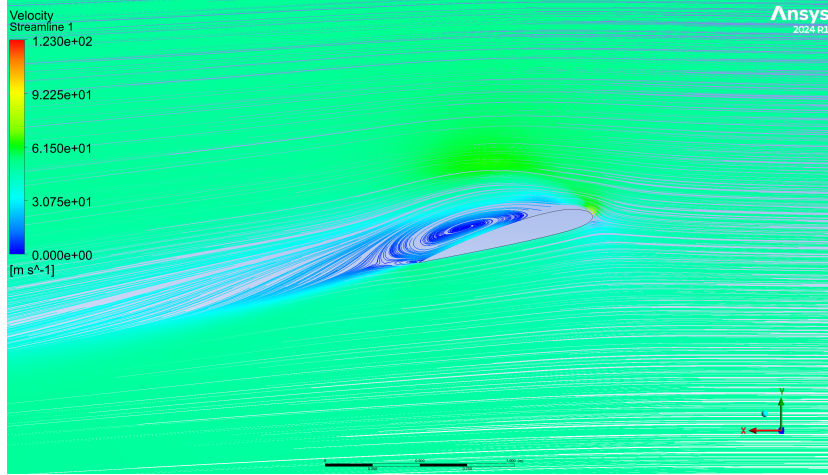


Figure 10: Streamline visualisation of the flow on a peak of a sinusoidal serrated airfoil with properties $\lambda/c = 0.1$, $A/c = 0.05$ and $d/c = 0.2$ with a flow velocity of $V = 50 \text{ ms}^{-1}$ at an AoA of $\alpha = 15^\circ$.

5 Conclusion

This interim report and project plan outlines the current work that has been completed on this research thesis into the aerodynamics of wings with LE serrations. The scope of the current literature has been outlined across all variable geometric properties of LE serrations, defining the value range that will be investigated in the latter stages of the project. The aerodynamic effect of LE serrations has been investigated, and the pre-stall and post-stall regimes have been characterised to define the focus of further investigations.

The aims and objectives of the project have been defined to answer the proposed research question. A detailed methodology has been created across two stages of a computational investigation and an experimental investigation. The computational investigations will utilise ANSYS Workbench for parametric studies of LE serraion properties using ANSYS Fluent for CFD simulations and ANSYS Design Modeller for AoA variation. UNSW's EWT will be used to experimentally investigate 3D printed models using the sting balance for aerodynamic force recording. The timeline of these investigations has been proposed, giving ample time to conduct thorough and effective computational simulations on UNSW's computational cluster Katana.

The design of the LE serrated wing has been completed, and preliminary CFD simulations have been run to determine the scope of the investigation, the dimensions of the fluid domain, and the mesh resolution and to verify the proof of concept of the aerodynamic effect of the LE serrations. The investigation has a clear path forward and will commence in the break of Term 1.

Acknowledgments

I would like to acknowledge my supervisor, Con Doolan, who has continually supported and aided me throughout this project and I would like to thank him for his future support as the project progresses.

References

- [1] Intizar Ali, Tanweer Hussain, Imran Nazir Unar, Laveet Kumar, and Inam Ul Ahad. Turbulence model study for aerodynamic analysis of the leading edge tubercle wing for low reynolds number flows. *Heliyon*, 10(11):e32148, 2024.
- [2] Rafael Bardera, Ángel Antonio Rodríguez-Sevillano, Estela Barroso-Barderas, and Juan Carlos Matías-García. Cfd study of the effect of leading-edge tubercles on the aerodynamic characteristics of a small uav based on eppler 186 airfoils. *Results in Engineering*, 23:107–129, 2024.
- [3] Jonathan Borg. The effect of leading edge serrations on dynamic stall. *University of Southampton, Faculty of Engineering and Environment*, 2012.
- [4] A. Esmaeili, H. E. C. Delgado, and J. M. M. Sousa. Numerical simulations of low-reynolds-number flow past finite wings with leading-edge protuberances. *Journal of Aircraft*, 55(1):226–238, 2018.
- [5] Irelyn Fernandes, Yogesh Sapkota, Tania Mammen, Atif Rasheed, Calvin Rebello, and Young Hwan Kim. Theoretical and experimental investigation of leading edge tubercles on the wing performance. *AIAA Journal*, 2013.
- [6] Franke E. Fish and Juliann M. Battle. Hydrodynamic design of the humpback whale flipper. *Journal of Morphology*, 225(1):51–60, 1995.
- [7] Kristy L. Hansen, Richard M. Kelso, and Bassam B. Dally. Performance variations of leading-edge tubercles for distinct airfoil profiles. *AIAA Journal*, 49(1):185–194, 2011.
- [8] Kristy Lee Hansen. Effect of leading edge tubercles on airfoil performance. *University of Adelaide, School of Mechanical Engineering*, 2012.
- [9] Ruixuan He, Xinjing Wang, Jian Li, Xiaodong Liu, and Baowei Song. Effects of leading-edge tubercles on three-dimensional flapping foils. *Journal of Marine Science and Engineering*, 11(10), 2023.
- [10] Jeena Joseph and A. Sathyabhama. Leading edge tubercle on wind turbine blade to mitigate problems of stall, hysteresis, and laminar separation bubble. *Energy Conversion and Management*, 255:115–137, 2022.
- [11] Manideep J.S.S, Levin Curtis Nixon, Koganti Naga Sai Ramu, and Ranjitha Eswaran. Effects of leading-edge tubercles and dimples on a cambered airfoil and its performance. *IRJET*, 9, 2022.
- [12] Auris Juknevicius and Tze Pei Chong. On the leading edge noise and aerodynamics of thin aerofoil subjected to the straight and curved serrations. *Journal of Sound and Vibration*, 425:324–343, 2018.
- [13] Wenliang Ke, Islam Hashem, Wenwu Zhang, and Baoshan Zhu. Influence of leading-edge tubercles on the aerodynamic performance of a horizontal-axis wind turbine: A numerical study. *Energy*, 239:122186, 2022.

- [14] Giovanni Lacagnina, Paruchuri Chaitanya, Jung-Hoon Kim, Tim Berk, Phillip Joseph, Kwing-So Choi, Bharathram Ganapathisubramani, Seyed Mohammad Hasheminejad, Tze Pei Chong, Oksana Stalnov, Muhammad Farrukh Shahab, Mohammad Omidyeganeh, and Alfredo Pinelli. Leading edge serrations for the reduction of aerofoil self-noise at low angle of attack, pre-stall and post-stall conditions. *International Journal of Aeroacoustics*, 20(1-2):130–156, 2021.
- [15] Hardeep Lall, Jaitra Khanna, Harsh Khatri, Sahil Mhapankar, Parmeshwar Paul, Anjali Vyas, and Student. Effect of tubercles on aerodynamic performance of naca 0015. *IRJET*, 6(3), 2008.
- [16] Kang Liu, Bifeng Song, Dong Xue, Wenqing Yang, Ang Chen, and Zhihe Wang. Numerical study of the aerodynamic effects of bio-inspired leading-edge serrations on a heaving wing at a low reynolds number. *Aerospace Science and Technology*, 124:107–129, 2022.
- [17] Mark Lohry, Luigi Martinelli, and David Clifton. Characterization and design of tubercle leading-edge wings. In *ICCFD7*, 2012.
- [18] David Miklosovic, M. Murray, Laurens Howle, and Frank Fish. Leading-edge tubercles delay stall on humpback whale (megaptera novaeangliae) flippers. *Physics of Fluids*, 16, 2004.
- [19] Weichao Shi Moritz M. F. Troll and Callum Stark. The influence of leading-edge tubercles on wake flow dynamics of a marine rudder. *Department of Naval Architecture, Ocean and Marine Engineering (NAOME)*, 2021.
- [20] Nikan Rostamzadeh, Richard Kelso, Bassam Dally, and Kristy Hansen. The effect of undulating leading-edge modifications on naca 0021 airfoil characteristics. *Physics of Fluids*, 25, 2013.
- [21] A. Sathyabhama and B. K. Sreejith. Numerical investigation on the effect of leading-edge tubercles on the laminar separation bubble. *Journal of Applied Fluid Mechanics*, 15(3):767–780, 2022.
- [22] Oksana Stalnov and Tze Pei Chong. Scaling of lift coefficient of an airfoil with leading-edge serrations. *AIAA Journal*, 57(8):3615–3619, 2019.
- [23] S. Sudhakar, N. Karthikeyan, and L. Venkatakrishnan. Influence of leading edge tubercles on aerodynamic characteristics of a high aspect-ratio uav. *Aerospace Science and Technology*, 69:281–289, 2017.
- [24] Dian Wang, Chang Cai, Rongyu Zha, Chaoyi Peng, Xuebin Feng, Pengcheng Liang, Keqilao Meng, Jianyu Kou, Takao Maeda, and Qing'an Li. Impact of leading-edge tubercles on airfoil aerodynamic performance and flow patterns at different reynolds numbers. *Energies*, 17(21), 2024.
- [25] Zhaoyu Wei, J.W.A. Toh, I.H. Ibrahim, and Yanni Zhang. Aerodynamic characteristics and surface flow structures of moderate aspect-ratio leading-edge tubercled wings. *European Journal of Mechanics - B/Fluids*, 75, 2019.
- [26] Yinan Zhang, Huijing Cao, Xia Liu, and Liangwen Qi. Effect of the leading-edge protuberances on the aeroacoustic and aerodynamic performances of the wind turbine airfoil. *Ocean Engineering*, 266:113–153, 2022.

Appendix

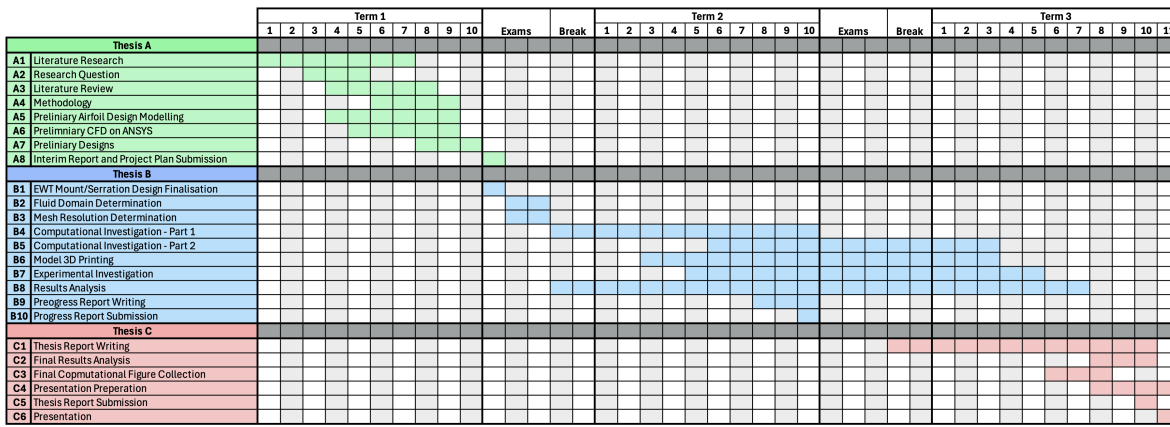


Figure 11: Gantt Chart of the proposed week-to-week timeline of the project.